

Artemisinin Cocrystals for Bioavailability Enhancement: Part 1. Formulation Design and Role of the Polymeric Excipient

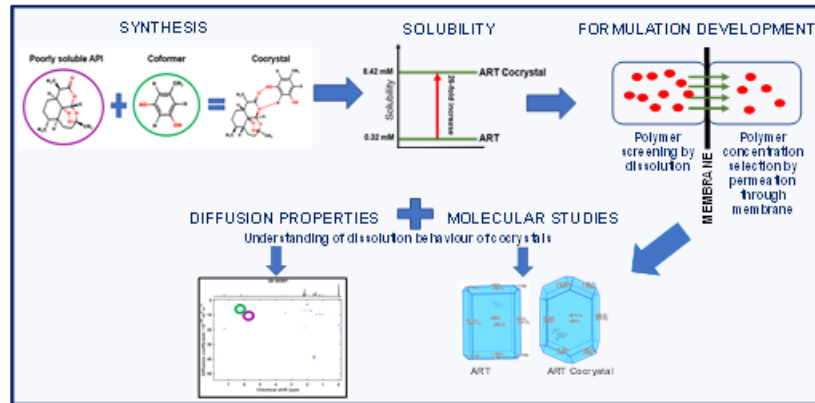
*Manreet Kaur¹, Vanessa Yardley², Ke Wang¹, Jinit Masania¹, Adolfo Botana³, Randolph RJ
Arroo¹ and Mingzhong Li^{*1}*

¹Leicester School of Pharmacy, De Montfort University, Leicester LE1 9BH, U.K.

²Department of Infection & Immunity, Faculty of Infectious & Tropical Diseases, London
School of Hygiene and Tropical Medicine, London, WC1E 7HT, U.K.

³JEOL (U.K.) LTD., Welwyn Garden City, AL7 1LT, U.K.

Table of Contents Graphic



Abstract:

Artemisinin (ART) is a most promising antimalarial agent, which is both effective and well-tolerated in patients, though it has therapeutic limitations due to its low solubility, bioavailability and short half-life. The objective of this work was to explore the possibility of formulating ART cocrystals, i.e., artemisinin-orcinol (ART-ORC) and artemisinin-resorcinol (ART²-RES) as oral dosage forms to deliver ART molecules for bioavailability enhancement. This is the first part of the study, aiming to develop a simple and effective formulation which can then be tested on an appropriate animal model (i.e. mouse selected for *in vivo* study) to evaluate their preclinical pharmacokinetics for further development. In the current work, the physicochemical properties (i.e., solubility and dissolution rate) of ART cocrystals were measured to collect information necessary for the formulation development strategy. It was found that the ART solubility can be increased significantly by its cocrystals, i.e., 26-fold by ART-ORC and 21-fold by ART²-RES respectively. Screening a set of polymers widely used in pharmaceutical products, including Polyvinylpyrrolidone, Hydroxypropyl Methylcellulose and Hydroxypropyl Methylcellulose Acetate Succinate, based on the powder dissolution performance parameter analysis, revealed that Polyvinylpyrrolidone/vinyl Acetate (PVP-VA) was the most effective crystallisation inhibitor. The optimal concentration of PVP-VA at 0.05 mg/mL for the formulation was then determined by a dissolution/permeability method which represented a simplified permeation model to simultaneously evaluate the effects of a crystallization inhibitor on the dissolution and permeation performance of ART cocrystals. Furthermore, experiments, including surface dissolution of single ART cocrystals monitored by Raman spectroscopy and SEM and diffusion properties of ART in solution measured by ¹H and diffusion-ordered spectroscopy (DOSY) nuclear magnetic resonance (NMR)

spectroscopy, provided insight into how the excipient affects the ART cocrystal dissolution performance and bioavailability.

Keywords: Artemisinin cocrystals, solubility, diffusion, bioavailability, ^1H NMR, and diffusion-ordered spectroscopy (DOSY)

Introduction

Malaria is a life-threatening disease caused by *Plasmodium* parasites that are transmitted to humans through the bites of infected female *Anopheles* mosquitoes. Malaria is a problem in every region of the developing world, particularly in Africa where over 90 percent of malaria cases and deaths occur [1]. The disease affects all ages and economic groups with a devastating impact particularly on pregnant women and children under five years old, and contributes significantly to mortality, poverty and underdevelopment in endemic regions [2]. Artemisinin (ART) is the most promising antimalarial agent, which is both effective and well tolerated in patients, however it has therapeutic limitations due to its low solubility, bioavailability and short half-life. [3]. To overcome these problems, several semisynthetic derivatives and fully synthetic analogues have been developed, such as artemether, arteether, dihydroartemisinin and artesunate [4]. These compounds have greater hydrolytic stability, lower toxicity, but have limited metabolic stability, drug resistance and high costs [4, 5].

ART has several dosing routes including oral, intramuscular, intravenous and rectal [3, 5, 6]. Because ART itself is a highly crystalline compound that does not dissolve in oil or water, and undergoes extensive first-pass metabolism, oral administration of ART is not the route of choice and its bioavailability is extremely low, i.e. 8-10% [7]. Furthermore, this low efficacy of ART after oral administration can aggravate the problem of resistance through incomplete parasite clearance. Therefore, an urgent need exists to develop oral formulations that can improve the therapeutic efficacy of ART, which has been ignored over the past decades.

Pharmaceutical cocrystallization has emerged as a new strategy to enhance the clinical performance of orally administered drugs [8]. Pharmaceutical cocrystals of active pharmaceutical ingredients (APIs) represent a class of multi-component crystalline forms that are of interest for their advantageous physical properties and for intellectual property implications [9-11]. By diversifying the number of cocrystal formers (i.e. cofomer) that exist

for a particular API, cocrystals can lead to improvements in solubility, dissolution rate, physical and chemical stability as well as in mechanical properties. Cocrystal design requires changes in crystal structures that essentially alter hydrogen bonding motifs rather than covalent bonds of the API, thus retaining its safety and therapeutic properties. Cocrystals of APIs are particularly attractive when salt formation is infeasible or when existing salts fail to exhibit suitable properties, such as weakly ionizable or non-ionizable molecules. In fact, ART is such a molecule; it is a sesquiterpene lactone containing an internal peroxide bridge, and does not form a salt due to its lack of ionisable sites (see Table 1). A large scale ART cocrystal screening involving 75 potential cofomers led to the discovery of two ART cocrystals [12]. ART forms 1:1 cocrystal with orcinol (ART-ORC) and 2:1 cocrystal with resorcinol (ART²-RES) via a synthon consisting of an O–H...O hydrogen bond between the OH group of ORC or RES and the carbonyl moiety of ART (see Table 1). The ART cocrystals can alter the melting points of ART, i.e., the melting points of ART-ORC and ART²-RES are 110°C and 103°C respectively in comparison with that of ART between 152°C and 157°C depending on its polymorphs [12]. However, it is not clear whether these two ART cocrystals can lead to improvement in the biopharmaceutical properties (i.e., solubility, dissolution rate, stability and permeability) of ART because the high potential of cocrystals to fine-tune physicochemical properties of APIs does not always lead to modulation of drug pharmacokinetics [8].

Although cocrystal approach itself seems straightforward, actual development of an effective formulation is challenging. The major hurdles encountered for cocrystal formulation development include unpredictable cocrystal performance during dissolution and solubility in different media, difficulties in establishing *in vitro-in vivo* correlation, and selection of excipients. A supersaturated solution concentration of the parent drug can be generated due to rapid dissolution of cocrystals, which is a key requirement for improved drug oral absorption

[13]. It is thus critical to include a polymeric excipient in the formulation as an inhibitor to prevent the parent drug crystallization and to maintain drug in solution in aqueous media for a sufficient length of time to allow absorption [14-18]. Selection of a polymeric excipient in a cocrystal formulation can be problematic because the interplay of the polymer with both the parent drug and coformer in solution could lead to erratic drug release performance *in vitro* or *in vivo* [19, 20]. Therefore, a thorough understanding of the dissolution mechanisms of cocrystals and their possible interaction with the excipients and dissolution environments is required to guide preclinical formulation development [21, 22].

The objective of this work was to design oral formulations of ART cocrystals which can be used on an appropriate rodent model (i.e. mouse selected for *in vivo* study) in order to evaluate their preclinical pharmacokinetics for further development. A simple and effective formulation, that allows ART cocrystals suspended in solution to be administered to mice, was developed. The physicochemical properties (i.e., solubility and dissolution rate) of ART cocrystals were measured to collect information necessary for a formulation development strategy. Screening of an effective excipient as a crystallisation inhibitor was drawn from a set of polymers widely used in pharmaceutical products, including Polyvinylpyrrolidone (PVP), copolymer Polyvinylpyrrolidone/vinyl Acetate (PVP-VA), Hydroxypropyl Methylcellulose (HPMC) and Hydroxypropyl Methylcellulose Acetate Succinate (HPMC-AS) (Table 1), using the powder dissolution performance parameter (DPP) analysis [19, 21]. The optimal concentration of the selected polymer in solution was determined by a dissolution/permeability (D/P) method [19, 20]. The D/P system represented a simplified permeation model to simultaneously evaluate the effects of a crystallization inhibitor on the dissolution and permeation performance of ART cocrystals in a formulation. Furthermore, experiments, including surface dissolution of single ART cocrystals monitored by Raman spectroscopy and SEM (scanning electron microscope) and diffusion properties of ART in

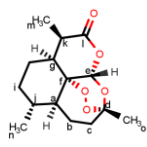
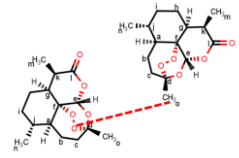
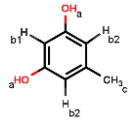
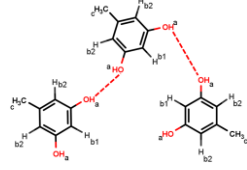
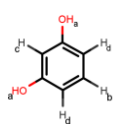
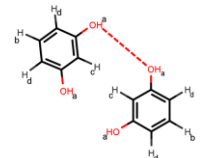
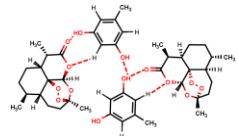
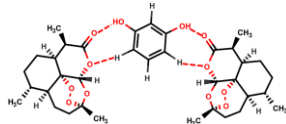
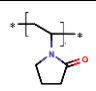
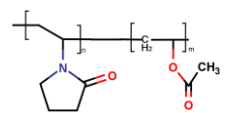
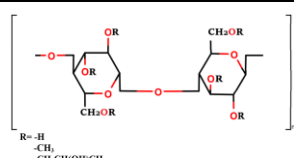
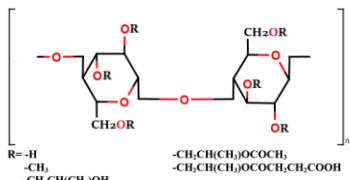
solution measured by ^1H and diffusion-ordered spectroscopy (DOSY) nuclear magnetic resonance (NMR) spectroscopy, were conducted to gain insight into how the excipient affects the ART cocrystal dissolution performance and bioavailability [20, 21].

Materials and Methods

Materials

Artemisinin (ART, 98% purity), resorcinol (RES, >99% purity), potassium dihydrogen phosphate (KH_2PO_4), santonin and sodium hydroxide (NaOH) were purchased from Sigma-Aldrich (Dorset, UK). Orcinol (ORC, 98% purity) was purchased from Fisher Scientific (Loughborough, UK). Polyvinylpyrrolidone K-29/32 (PVP), copolymer polyvinylpyrrolidone/vinyl acetate (PVP-VA), hydroxypropyl methylcellulose K4M Pharm Benecel (HPMC) and hydroxypropyl methylcellulose acetate succinate (Medium grade, HPMC-AS) were gifts from Ashland Inc (Schaffhausen, Switzerland). HPLC and LCMS grade solvents including methanol, acetonitrile, water and formic acid were purchased from Fisher Scientific and used as received. Double distilled water (DDW) was generated from a bi-distiller (WSCO44.MH3.7, Fistreem International Limited, Loughborough, UK) and used throughout the study. Electrospray tuning mix for LC-MS was purchased from Agilent Technologies Ltd (Cheshire, UK).

Table 1: Chemical structures of cocrystal components and monomer units of polymers

	Molecular structure	Supramolecular synthons	Molar weight (Da)
ART			282.332
ORC			124.13
RES			110.1
ART-ORC CO			406.46
ART ² -RES CO			674.76
PVP			40,000
PVP-VA			51,000
HPMC	 R = -H -CH ₃ -CH ₂ CH(OH)CH ₂		400,000
HPMC-AS	 R = -H -CH ₃ -CH ₂ CH(CH ₂)OH -COCH ₃ -COCH ₂ CH ₂ COOH		103,200

Methods

Phosphate buffer solution (PBS)

PBS at pH 6.8 (0.01M) was used for solubility experiments and as dissolution media in this study. It was prepared according to the British Pharmacopeia 2018; 50mL of 0.2M KH_2PO_4 and 22.4mL of 0.2M NaOH were mixed and diluted to 1000mL with double distilled water. 0.01M pH 4.5 PBS was prepared using the same approach to study the pH dependent solubility properties of ART.

Preparation of powdered ART cocrystals

Artemisinin and orcinol cocrystal (ART-ORC) was prepared by solvent evaporation method. A 1:1 equimolar mixture of ART and ORC was dissolved in the solvent mixture of chloroform and methanol (9:1) at room temperature. The solution was placed in a fume cabinet (room temperature, air flow 0.5-1.0 m/s) for 4-5 days to let the solvents evaporate.

Artemisinin and resorcinol cocrystal (ART²-RES) was synthesized by seeded solvent evaporation methods. A 2:1 molar mixture of ART and RES was used to prepare the seeds of cocrystals by a neat grinding method using Retsch Mixer Mill MM 400 (Retsch, Germany) along with 15mL stainless steel SmartSnapTM jars containing two 7 mm stainless steel grinding balls (Form-tech Scientific, Montreal, Canada) for 60 min. The neat grinded cocrystals were then used as seeds to prepare enough quantity of ART²-RES needed for experiments by solvent evaporation method, where 2:1 molar ratio mixture of both components was present in a saturated cosolvent solution of chloroform and methanol (9:1). The cocrystal solutions were allowed to evaporate in a controlled fume hood for 4-5 days.

Single ART cocrystal preparation, morphology prediction, face indexing and etching dissolution experiments

Single crystal of ART was directly selected from the commercial products while the single ART cocrystals were grown by addition of powdered cocrystal seeds in saturated mixture solutions of ART and cofomers (1:1 ART-ORC and 2:1 ART²-RES), where a cosolvent mixture of chloroform and methanol at ratio of 9:1 was used, by slow evaporation at room

temperature over a period of 12-15 days. ART cocrystals were harvested by gravity filtration of the mother solutions.

The morphology of each of the single crystals i.e., ART, ART-ORC, ART²-RES, was created using Mercury CSD 4.1.2 [The Cambridge Crystallographic Data Centre (CCDC), Cambridge, UK]. The structures of the unit cell of single crystals were obtained from Cambridge Structural Database (CSD) (reference codes QNGHSU03 for ART; TALCUG for ART-ORC and TALCOA for ART²-RES). The predicted morphologies of the crystals were validated by comparing the PXRD patterns from the DASH module of CCDC with the experimental measurements.

The index of a single crystal face was determined by the face specific PXRD patterns through comparing the observed crystal shape with the simulated morphology. Each single crystal was mounted onto the PXRD specially designed single crystal sample holder and the face-specified measurements were then compared with the simulated PXRD patterns.

Single crystals with well-defined faces were selected under a microscope for the etching dissolution experiments. A single crystal was first mounted onto a cover slip using double-sided seal tape, where the studied face was up and exposed. The cover slip was then immersed for 2 min in a petri dish which contained 20mL of pre-heated (at 37°C) 0.01M pH 6.8 PBS in the absence or presence of the selected polymer as shown in [22]. The cover slip was taken out from the solution after a pre-determined time interval and the remaining solution on the crystal surface was removed with filter paper. Finally, the sample was air-dried for at least 1h before analyzing under Raman Spectroscopy and SEM.

Table 2: Time Interval for etching dissolution experiments

Crystal	(Face index)/ 2 θ on PXRD pattern	Dissolution time (min)		
		PBS	PBS with pre-dissolved PVP-VA of 0.05 mg/mL	PBS with pre-dissolved PVP-VA of 0.5 mg/mL
ART	(0,0,2)/7.4°	2	2	2
ART-ORC	(0,1,1)/8.1°	2	2	2
ART ² -RES	(0,2,0)/10.1°	2	2	2

Solubility studies

The solubility of ART was measured by suspending an excess amount of ground powder with particle size <250 μ m into a vial with 20mL of DDW, 0.01M pH 4.5 PBS or 0.01M pH 6.8 PBS in a shaking water bath at 150 rpm shaking rate and 37 \pm 0.5°C for 24 h. Then, suspended particles were separated by centrifugation in an MSC 010.CX2.5 centrifuge (MSE Ltd., London, UK) at 13,000rpm for 1 min. The test was repeated in triplicates and the ART concentration in the supernatant was determined by HPLC.

For a m:n cocrystal of AB without considering the ionisation of each component, its molar solubility is calculated as [23],

$$S_{AB} = {}^{m+n}\sqrt{K_{sp}} = {}^{m+n}\sqrt{A_{eu}^m B_{eu}^n} \quad (1)$$

where K_{sp} is the solubility product of the $A_m B_n$ cocrystal and concentrations of A_{eu} and B_{eu} are transient molar concentrations of drug and coformer where the solution is in equilibrium with solid drug and cocrystal.

The ratio R_{CO} of a cocrystal solubility via its parent drug A is calculated by

$$R_{CO} = \frac{S_{AB}}{S_A} \quad (2)$$

where S_A is the molar solubility of the parent drug A.

In order to measure the transition concentrations of ART and a coformer of ORC or RES in PBS, a series of coformer solutions were prepared: 0, 32.2, 128.8, 161.1, 177.2, 241.6 330.2 mM for ORC solutions and 0, 36.3, 145.3, 272.4, 290.6, 308.8, 544.9, 726.6 and 908.2 mM for RES solutions. Excess amount of ART ground material (particle size of <250 μ m) was

added into a vial with 20mL of each of the prepared coformer solutions in a shaking water bath at 150 rpm shaking rate and $37 \pm 0.5^\circ \text{C}$ for 24 h. The concentrations of ART and coformer of ORC or RES were determined by HPLC and the solid residues retrieved were analysed by PXRD. The transition concentrations (or eutectic point) of a cocrystal were determined in the lowest coformer solution prepared where two solid phases of the solid drug and cocrystal existed in equilibrium with solution. All experiments were done in triplicates.

Screening of polymers by powder dissolution studies

The polymers used for screening included HPMC, HPMC-AS, PVP and PVP-VA at a fixed concentration of 0.1mg/mL in the dissolution medium. A dissolution test was carried out in non-sink conditions where dissolution medium was pH 6.8 PBS in absence or presence of a pre-dissolved polymer of 0.1mg/mL. In order to reduce the effect of particle size on the dissolution rates, ART, ART-ORC and ART²-RES samples were ground using 60Mesh Sieve to obtain a particle size of $<250\mu\text{m}$. The experiments were carried out at $37 \pm 0.5^\circ\text{C}$ in a PTWS 120D dissolution apparatus (PharmaTest, Germany) at 50rpm stirring speed. The total volume of dissolution media was 400mL, in which 150mg of ART, 215.9mg of ART-ORC and 179.3mg ART²-RES was added. 1mL sample was withdrawn at sampling intervals of 5, 10, 15, 30, 60, 120, 180 and 240 min. The withdrawn sample was centrifuged using MSC 010.CX2.5 centrifuge (MSE Ltd., London, UK) at 13,000rpm for 1 min. The supernatant was separated, diluted with ethanol and the concentrations were detected using HPLC. All experiments were done in triplicates.

Optimal polymer concentration determination by dissolution/permeability (D/P) measurements

The optimal concentration of the selected polymer as a crystallization inhibitor was determined by a D/P system which was used to evaluate the dissolution and permeation performance of cocrystals simultaneously detailed in our previous publication [20]. Briefly, it consisted of a donor and an acceptor compartment, which was separated by a regenerated

cellulose membrane with a molecular weight cut-off (MWCO) of 6-8 kDa (Spectrum Laboratories Inc. Rancho Dominguez CA 90220, USA). Both donor and acceptor compartments have a capacity of 10mL. The orifice diameter of the compartment was 0.9cm, corresponding to 0.671 cm² surface area of the membrane. All powder samples for this part of the study had particle size no bigger than 250 μm. Either 5 mg of single component crystals of ART or cocrystals with an equivalent amount of ART were first added to the donor compartment, followed by the addition of 9 mL of DDW to the acceptor compartment. Then, 9 mL of 0.01 M PBS (pH 6.8) in the absence or presence of the polymer obtained by the screening experiments above was added to the donor compartment that contained the crystals. Three polymer concentrations, i.e., 0.1, 0.05 and 0.01 mg/mL, were selected in the study. The temperature of the whole system was maintained at 37 ± 0.5 °C by a circulating water bath. 0.5 mL of sample was withdrawn from the donor compartment at the time intervals of 5, 10, 15, 30, 60, 120, 180 and 240 min using a syringe, and any volume change due to the withdrawal was immediately compensated with fresh dissolution medium of the same temperature i.e. 37 ± 0.5 °C. 0.5 mL of the non-replaceable solution was withdrawn from the acceptor side at 30, 60, 120 and 240 min. All experiments were done in triplicates.

The concentrations of ART, ORC and RES from donor chamber were determined using HPLC and ART concentration from acceptor compartment was determined using LC-MS. The cofomer concentrations from acceptor side were detected on HPLC.

High Performance Liquid Chromatography (HPLC) methods for ART, ORC and RES

The sample concentration of ART, ORC or RES in solution was determined by Agilent series 1100 automatic HPLC equipped with a diode array detector. A Roc C18 column (5 μm, 150 x 4.6 mm, Restek) was used and the column temperature was maintained at 25 °C. Details of HPLC methods are shown in Table 3.

Table 3: HPLC methods

Component	Mobile Phase		Flow rate (mL/min)	Injection volume (μ L)	Detection Wavelength (nm)	Retention time (min)
ART	25% Acetonitrile	75% mixture of Water and Methanol (3:2)	0.5	50	206	33
ORC	30% Methanol	70% Water with 0.1% formic acid	0.5	20	280	10
RES	30% Methanol	70% Water with 0.1% formic acid	0.5	20	270	8

The ART calibration samples were prepared in acetonitrile in a range of 5 - 50 μ g/mL. Both ORC and RES calibration samples were prepared in DDW in a range of 5 - 50 μ g/mL. The validation solutions were 15 and 25 μ g/mL for ART; 20 and 45 μ g/mL for ORC; 15 and 45 μ g/mL for RES (detailed Table S1 in the supplementary materials).

Liquid Chromatography- Mass Spectrometry (LC-MS) method for ART

In a D/P experiment, ART solution concentration in the acceptor cell was too low to be detected by the HPLC method above. Therefore, a LC-MS method was developed to detect the ART concentration in solution, using Agilent Technologies 1260 Infinity system coupled to an Agilent Technologies 6120 Quadrupole mass spectrometer, accompanying with its OpenLab CDS Chemstation Edition C.01.09 software for data acquisition and analysis (Agilent Technologies Ltd, Cheshire, UK). The LC separation was achieved with an isocratic mobile phase of 50% acetonitrile; and 50% water and methanol mixture (3:2 ratio) with a flow rate of 0.5 mL/min on a Roc C18 column (5 μ m, 150 x 4.6 mm, Restek). Details of LCMS method are shown in Table 4. MS with electrospray ionisation in positive mode was used with single ion monitoring. The spray chamber and mass spectrometer parameters were as follows: nitrogen flow at 12 L m⁻¹; drying gas temperature 350 °C; capillary voltage 3400 V in positive mode, 3000V in negative mode; nebulizer pressure 50 psig; and fragmentor

voltage 50 V. The mass spectrometer was calibrated and tuned regularly using Agilent's Electrospray Tuning Mix, to ensure peak performance.

Table 4: LC-MS method

Components	Mobile Phases		Flow rate (mL/min)	Injection volume (μ L)	Ion monitored (m/z)	Retention time (min)
	50% Acetonitrile	50% Water and Methanol mixture (3:2)				
ART	50% Acetonitrile	50% Water and Methanol mixture (3:2)	0.5	20	283.3	6.8
SAN (IS)	-	-	-	-	247.3	4.4

The molecular ion m/z 283.3 and m/z 247.3 was monitored for ART and santonin (SAN; internal standard) respectively. A calibration curve was generated with ART concentration ranged from 0.1 to 20 μ g/mL. The validation solutions were concentrations of 2, 4 and 12 μ g/mL. In order to prepare working solutions, SAN with constant concentration of 1 μ g/mL, prepared in acetonitrile was added. Therefore, the working solutions were in the range of 0.05 to 10 μ g/mL and validation solutions tested were 1, 2 and 6 μ g/mL (2 times dilution with SAN). The injection sample volume was 20 μ l and all samples were analysed three times. The ratio of ART to SAN was calculated for each analysis; linear regression of the resulting scatter plot was used to establish the calibration curve. The retention time achieved was 6.8 min and 4.4 min for ART and SAN respectively. Details can be found in Table S2 in the supplementary materials.

¹H and diffusion ordered spectroscopy (DOSY) nuclear magnetic resonance (NMR)

¹H NMR was used to identify the interactions amongst the API, cofomer and polymer in solution and ART's diffusion properties were studied by conducting DOSY NMR experiments. The measurements were carried out with a JEOL ECZ600R MHz NMR Spectrometer (JEOL Limited, Hertfordshire, UK). The settings were kept the same for all measurements for each type of experiments, i.e., ¹H or DOSY.

The parameters for ^1H NMR experiments included 64 scans with a relaxation delay of 5 s and probe temperature of 25 °C. The diffusion measurements were bipolar pulse pair double stimulated echo sequence with convection compensation, non-spinning with a diffusion delay of 0.1 s and relaxation delay of 6 s. The probe temperature was maintained at 25 °C and gradient strength varied from 30 to 300 (mT/m) spaced equal steps of gradient square. The ^1H NMR data was analysed using MestReNova Version 12.0 (Mestrelab Research, Escondido, CA 92027, USA) software and DOSY data was analysed using General NMR Analysis Toolbox (GNAT, University of Manchester, UK). All samples were prepared in deuterated chloroform (CDCl_3), using the standard 5 mm NMR tubes and the spectra of tetramethylsilane (TMS, 0.05% v/v) was used as an internal standard. The measurements conducted included spectra of the singular components (ART, ORC, RES, PVP-VA), the binary components (ART/PVP-VA, ORC/PVP-VA, RES/PVP-VA, ART/ORC, ART/RES,) and the ternary components (ART/ORC/PVP-VA, ART/RES/PVP-VA). The ART concentration in each of solutions was constant at 1 mg/mL. In order to mimic a cocrystal system, the concentrations of ORC and RES were 0.43 mg/mL and 0.19 mg/mL in the solutions to achieve a 1:1 molar ratio of ART/ORC and 2:1 molar ratio of ART/RES. To investigate the effect of polymer on the simulated cocrystal system, PVP-VA was included in the solution at two different concentrations of 0.5 mg/mL and 1 mg/mL. Details of samples and preparation can be found in Table S3 in the supplementary materials.

Crystal characterization techniques

1) *Attenuated Total Reflection- Fourier Transform Infrared Spectroscopy (ATR-FTIR)*: FTIR spectra of the solid samples were measured using an ALPHA interferometer (Bruker U.K. Limited, Coventry, U.K.) with a horizontal universal attenuated total reflectance (ATR) accessory. The samples were placed on the surface of the diamond ATR plate and the ATR assembly was clamped to ensure good contact. In each measurement, 30 scans were collected

per spectrum with a resolution of 2 cm^{-1} in the spectral region of 400 to 4000 cm^{-1} using OPUS software.

2) *Differential Scanning Calorimetry (DSC)*: The melting point of solids was measured by a PerkinElmer Jade DSC (PerkinElmer Ltd, Beaconsfield, UK) controlled by Pyris software. The temperature and heat flow of the instrument were calibrated using indium and zinc standards. The sample (8-10 mg) was analyzed in a crimped aluminum pan with a pinhole pierced lid. The measurements were carried out at a heating rate of $20\text{ }^{\circ}\text{C}/\text{min}$ under a nitrogen gas with a flow rate of $20\text{ mL}/\text{min}$.

3) *Powder X-Ray Diffraction (PXRD)*: X-ray powder diffraction patterns of solids were recorded from 5° to 35° at a scanning rate of $0.3^{\circ} (2\Theta)\text{ min}^{-1}$ by a D2 PHASER diffractometer (Bruker UK Limited, Coventry, UK). Cu-K β radiation was used with a voltage of 30 kV and a current of 10 mA.

4) *Light microscope*: A LEICA DM 750 polarized light microscope (Leica Microsystem Ltd., Milton Keynes, UK) with a video camera at 200X magnification version 4.0 of the Studio Capture software was used to observe the single crystal shape.

5) *Raman Spectroscopy*: In this study, Enspectr R532[®] Raman Spectroscopy (Enhanced Spectrometry, Inc, Torrance, USA) was used to observe the surfaces of the single cocrystals to determine the precipitation behavior of the parent drug on any single cocrystal. In order to do that, the single cocrystal was placed inside the sample holder and scanned at RT, 20-30 mV output power, a wavelength of 532nm and wavenumber range of 100 to 4000 cm^{-1} . The Raman spectra of single crystal face before and after dissolution in presence or absence of polymer was recorded. An integration time of 300 milliseconds was fixed and each spectrum was achieved in an average of 700 scans.

6) *Scanning electron microscope (SEM)*: In this study, SEM micrographs were developed with a ZEISS EVO HD 15 scanning electron microscope (Carl Zeiss NTD Ltd., Cambridge

UK). SEM was used to determine the surface topology of the single cocrystal before and after dissolution. The single cocrystal was mounted on Agar Scientific G301 0.5" aluminum specimen stub (Agar Scientific Ltd., Stansted, UK) with Agar Scientific G3347N carbon adhesive tab and photographed at a voltage of 10.00kV. The manual sputter coating S150B was used for gold sputtering of the samples and the thickness of gold coating was 15 nm.

Results

ART cocrystal characterization

The formation of ART cocrystals was confirmed by PXRD, DSC and ATR-FTIR measurements.

A comparison of PXRD patterns of an ART cocrystal (i.e., ART-ORC or ART²-RES) with individual components confirmed the formation of new crystalline forms of ART cocrystals shown in Fig. 1. The characteristic peaks of ART are at $2\theta = 7.4^\circ, 11.9^\circ, 14.8^\circ, 15.7^\circ, 16.6^\circ, 18.4^\circ, 20.2^\circ$ and 22.2° [24]. Key characteristic diffraction peaks of ORC are at $2\theta = 8.7^\circ, 12.3^\circ, 14.6^\circ, 19.5^\circ, 21.1^\circ$ and 22.8° . ART-ORC exhibits a strong characteristic reflection at about $2\theta = 8.1^\circ$ and 14.3° and at the same time all characteristic peaks of ART and ORC disappeared, which is in good agreement with those of published data [12]. The characteristic peaks of RES are at $2\theta = 18.2^\circ, 19.2^\circ, 20.0^\circ, 20.3^\circ, 25.1^\circ$ and 29.7° . ART²-RES shows the characteristic peaks at $2\theta = 10.1^\circ, 10.7^\circ, 12.3^\circ, 13.2^\circ$ and 14.0° [12].

The DSC and FTIR results from characterization are discussed in Fig. S1 in the supplementary materials.

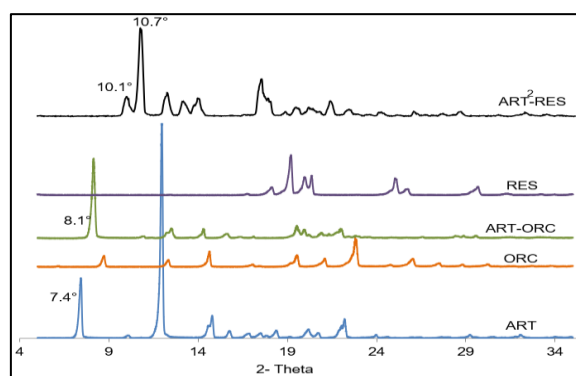


Fig. 1: Characterization of ART-ORC, ART²-RES and individual components using PXRD

ART cocrystal solubility studies

The apparent ART equilibrium solubility at 37 ± 0.5 °C was measured shown in Table 5. It is clearly indicated that the solubility of ART is pH independent, which was 92.3 ± 3.1 $\mu\text{g/mL}$ in DDW, 93.4 ± 0.9 $\mu\text{g/mL}$ in PBS pH 4.5 (0.01M) and 92.2 ± 1.2 $\mu\text{g/mL}$ in PBS pH 6.8 (0.01M).

The apparent concentration of ART as a function of ORC concentrations in solution after equilibration for 24 h shown in Fig. 2(a). The solubility of ART increased with increasing the ORC concentrations due to soluble complex formation between the two compounds. In solutions of an ORC concentration of 161.1 mM or above, the PXRD analysis of solid residues indicated the presence of two phases, ART-ORC and ART as shown in Fig. 2(b). Therefore, the measured concentrations of ART and ORC in 161.1 mM ORC solution represent the ART-ORC transition (Table 5). The molar ratio of ART to ORC at the transition point was 0.004:1. The solubility of ART-ORC was calculated as 8.4 mM using Eq. (1), which is a 26-fold increase compared to the solubility of ART alone.

The apparent concentration of ART as a function of RES concentrations is shown in Fig. 2(c). Similar to the ART-ORC solubility curve, the solubility of ART increased with increasing RES concentrations due to soluble complex formation between ART and RES in

solution. In solutions with a RES concentration of 290.6 mM or above, the solid residues indicated the presence of two phases: ART and ART²-RES, as confirmed by PXRD results in Fig. 2(d). The measured concentrations of ART and RES in 290.6mM RES solution represent the ART²-RES transition (Table 5). The molar ratio of ART to RES at the transition point was 0.003:1. The solubility of ART²-RES was calculated as 17.4 mM using Eq. (1), which is a 21-fold increase compared to the solubility of ART alone.

Based on the solubility test results, it would be expected that ART-ORC has a better performance than ART²-RES.

Table 5: Solubility Test Results

ART equilibrium solubility (µg/mL)	Double distilled water	92.3±3.1
	PBS pH 4.5 (0.01M)	93.4±0.9
	PBS pH 6.8 (0.01M)	92.2±1.2
ART-ORC cocrystal transition concentration (µg/mL)	ART concentration in 161.1 mM of ORC solution	158.7±6.1
	ORC concentration in 161.1 mM of ORC solution	15644± 431
	Solubility ratio R_{CO}	26
ART ² -RES cocrystal transition concentration (µg/mL)	ART concentration in 290.6mM of RES solution	301.4±6.7
	RES concentration in 290.6Mm of RES solution	31485±480
	Solubility ratio R_{CO}	21

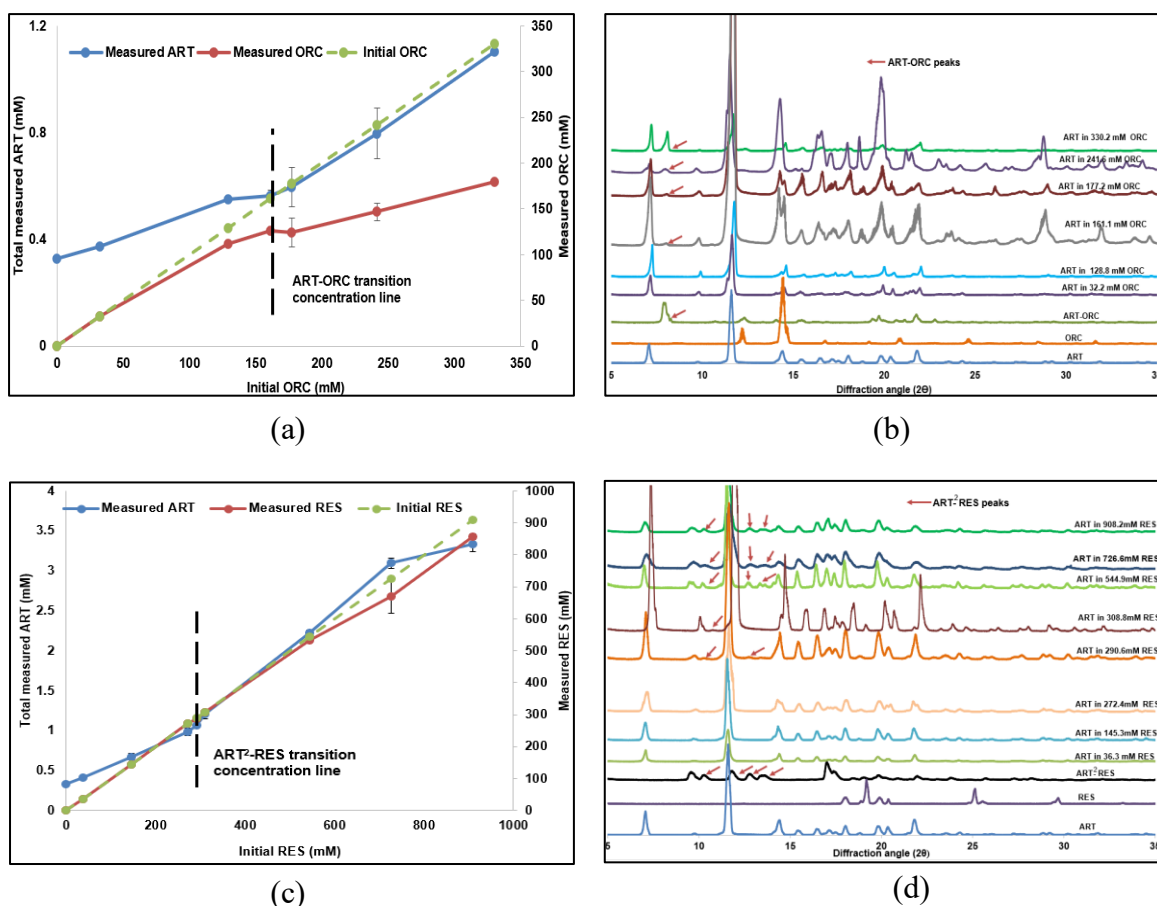


Fig. 2: Apparent solubility of ART in a coformer solution (a) ART and ORC concentrations as a function of ORC concentrations; (b) PXRD results of solid residues after the tests in ORC solutions; (c) ART and RES concentrations as a function of RES concentration; (d) PXRD results of solid residues after the tests in RES solutions

Formulation development

Aqueous suspensions were selected as a delivery vehicle to administrate the ART cocrystals because of their simplicity and effectiveness to evaluate both dissolution and permeation properties of the drug products in the animal test. To circumvent the recrystallisation problem of ART cocrystals in the vehicle, a polymeric excipient acting as crystallization inhibitor was required to be included into the delivery vehicle.

Determination of an effective polymer as crystallization inhibitor

In the polymer screening study, selection of a pre-dissolved polymer concentration of 0.1 mg/mL was based on the previous solubility study, which did not affect the equilibrium solubility of APIs [19]. The dissolution performance parameter (DPP) was used to evaluate

the dissolution profile of ART cocrystals in the absence or presence of a pre-dissolved polymer in comparison to a reference system of ART in PBS [19].

Figs. 3(a)-(e) show the dissolution profiles of ART, ART-ORC and ART²-RES in the absence and presence of a polymer, i.e. HPMC, HPMC-AS, PVP and PVP-VA, under non-sink conditions. In the presence of a polymer, ART solids dissolved slower shown in Fig. 3(f) as the reductions of areas under the curve (AUCs) are 11%, 26%, 23% and 34% for PVP, PVP-VA, HPMC and HPMC-AS, respectively.

ART-ORC and ART²-RES showed an advantage of improved dissolution relative to ART solids both in the absence or presence of a pre-dissolved polymer. In case of ART-ORC, pre-dissolved PVP-VA in solution shows the highest increase of DPP to 68% from 58% in PBS without a polymer. PVP shows a comparable effect as PVP-VA on the increase of DPP to 66%. In contrast, a pre-dissolved HPMC or HPMC-AS has shown a decrease in DPP as 48% or 39% respectively.

In case of ART²-RES, a pre-dissolved polymer of PVP-VA, PVP or HPMC shows a similar positive effect on increasing DPP, i.e., 46%, 44% and 42%, in comparison with 26% in pure PBS in the absence of a polymer. A very small increase of 26% was also observed in DPP in the presence of a pre-dissolved HPMC-AS.

Based on these results, PVP-VA was chosen as a crystallization inhibitor for ART cocrystals in the formulation.

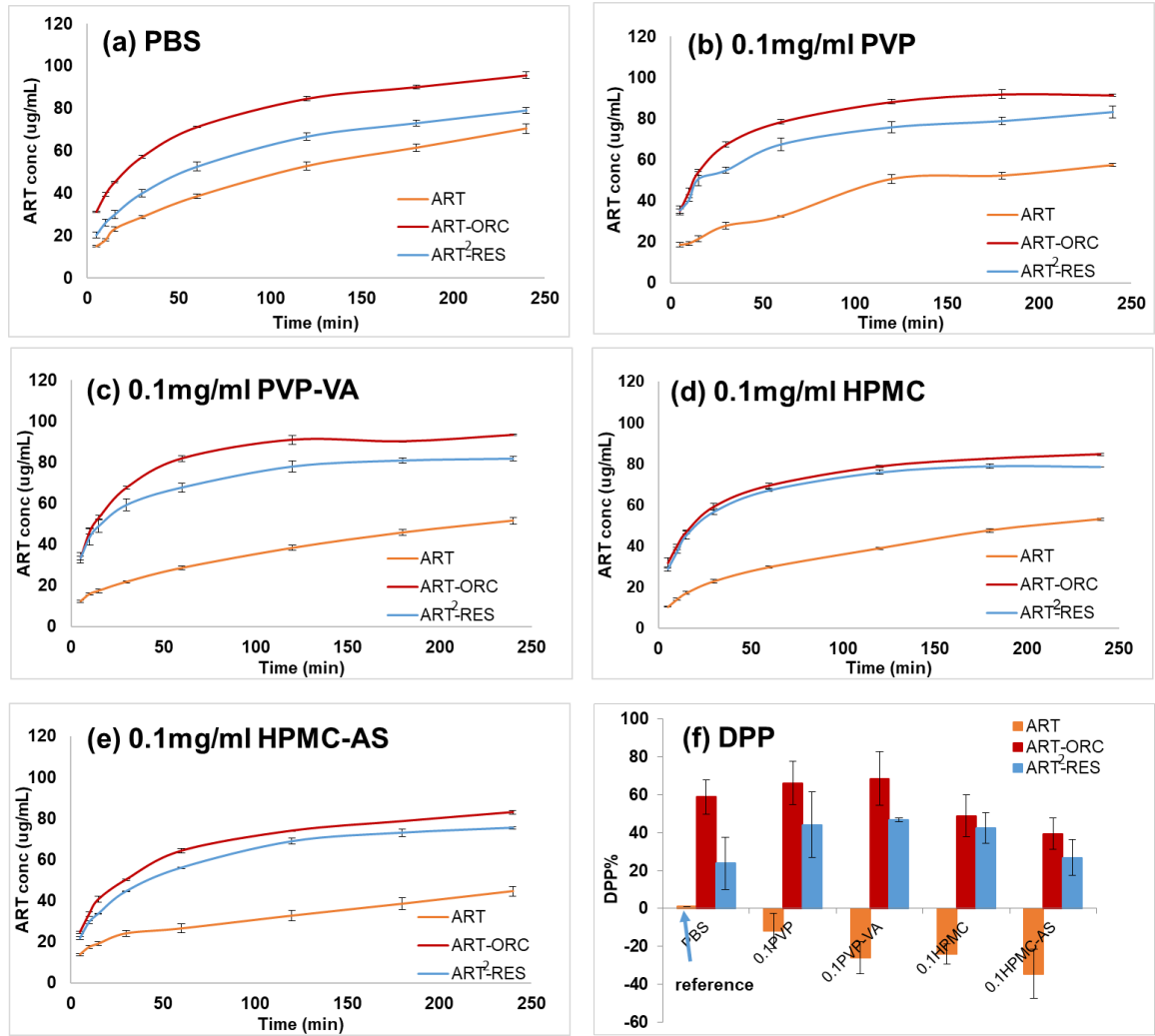


Fig. 3: Powder dissolution profiles in the absence or presence of a polymer under non-sink conditions: (a) PBS; (b) PBS with pre-dissolved 0.1mg/mL PVP; (c) PBS with pre-dissolved 0.1mg/mL PVP-VA; (d) PBS with pre-dissolved 0.1mg/mL HPMC; (e) PBS with pre-dissolved 0.1mg/mL HPMC-AS; (f) DPP comparison

D/P experiments to determine the optimal PVP-VA concentration

The optimal PVP-VA concentration was determined using D/P experiments where three different polymer concentrations, i.e., 0.1 mg/mL 0.05 mg/mL and 0.01 mg/mL, were pre-dissolved in PBS in the donor compartment. The DPP was used to evaluate the dissolution performance of the ART cocrystals in the donor compartment and the flux of ART through membrane into the acceptor compartment was calculated using the following equation [20]:

$$J(t) = \frac{(C_{t_2} - C_{t_1})}{A(t_2 - t_1)} V \quad (3)$$

where $J(t)$ stands for Flux rate, C_{t_1} is the drug concentration in the donor compartment at t_1 , C_{t_2} is the drug concentration in the donor compartment at t_2 , V is the solution volume of the donor compartment, and A is the area of exposed membrane.

The dialysis membrane acted as a selective barrier for the substances to pass through based on their sizes. The MWCO of the dialysis membrane used in this study was 6-8 kDa and it would thus allow the transfer of ART, which has a molecular weight (MW) of 282 Da, from the donor compartment into the acceptor compartment. The coformers (i.e., ORC and RES) have their MWs smaller than the pore size of the membrane and PVP-VA has its MW larger than the pore size of the membrane. Therefore, only ART and the coformers can pass through the membrane and not the polymer.

Fig.4(a1) shows the dissolution profiles of ART, ART-ORC and ART²-RES in PBS obtained from the D/P system. It can be seen that ART-ORC had the fastest dissolution rate and ART reached its solubility, 92 $\mu\text{g/mL}$ in 180min. ART concentration dissolved from ART²-RES achieved 89 $\mu\text{g/mL}$ after 4 h. In case of ART alone, the dissolution rate is the slowest as compared to the two ART cocrystals. The quantitative comparison of DPPs is shown in Fig.4(e) where ART-ORC had the highest value and followed by ART²-RES. Fig. 4(a2) shows the permeation profile of ART, ART-ORC and ART²-RES in PBS obtained from the D/P system. The ART concentrations in all three systems were very close to each other for the first 60 min of the experiment. Both ART cocrystals showed very similar permeation profiles and their permeation rates were higher as compared to the API alone. This was consistent with the mass flux rate as shown in Fig. 4 (f). ART-ORC showed a slightly higher ART influx rate as compared to ART²-RES.

Effects of different concentrations of a pre-dissolved PVP-VA in the donor compartment on the dissolution and permeation performances of ART, ART-ORC and ART²-RES are shown in Figs. 4(b1) -(d1).

The dissolution profiles show that dissolution rate of ART was enhanced in an ART cocrystal formulation, when the dissolution medium was PBS and increased further in presence of pre-dissolved PVP-VA, as compared to parent drug alone in the presence of the same concentrations of the polymer.

In case of PBS without polymer, the value of DPP achieved was 12% for ART-ORC. With addition of pre-dissolved 0.01 mg/mL PVP-VA in solution, the DPP remained same for ART-ORC as 12%. By increasing the pre-dissolved polymer concentration to 0.05 mg/mL, the DPP increased to 17% and further increasing the concentration of pre-dissolved polymer to 0.1mg/mL, highest DPP value was achieved of 29% for this particular cocrystal formulation.

The comparison of DPP was given in Fig. 4(e). The DPP value was approximately 1% for ART²-RES in PBS without polymer. With addition of pre-dissolved 0.01mg/mL PVP-VA, the DPP value of 6% was achieved and it did not further increase by addition of pre-dissolved polymer of 0.05 mg/mL. The DPP value increased slightly to 8% by increasing the polymer concentration up to 0.1 mg/mL.

The flux rate of both cocrystals increased slightly as compared to the drug alone, in absence of pre-dissolved polymer [Fig. 4(a2)]. However, due to the addition of a pre-dissolved polymer, the flux rate of both cocrystals increased significantly as compared to buffer without polymer. It was observed for both ART cocrystals that their flux rates were increasing with polymer concentrations of 0.01 mg/mL [Fig. 4(b2)] and 0.05 mg/mL [Fig. 4(c2)], in contrast, within 0.1 mg/mL polymer concentration solution, the flux rates of the two ART cocrystals started to reduce [Fig. 4(d2)]. The direct comparison of the diffusion flux rates was given in Fig. 4(f). The results showed that the flux rate of ART was dependent on the concentration of the pre-dissolved polymer. It was observed that the solution viscosity at the highest polymer concentration of 0.1 mg/mL did not change significantly. Therefore, the strength of

interactions between the drug/polymer/coformer could play a key role to affect the drug flux rate to the acceptor chamber, which was studied by the DOSY measurements.

Based on the study above, the optimal concentration of a pre-dissolved PVP-VA should be set as 0.05 mg/mL in the formulation.

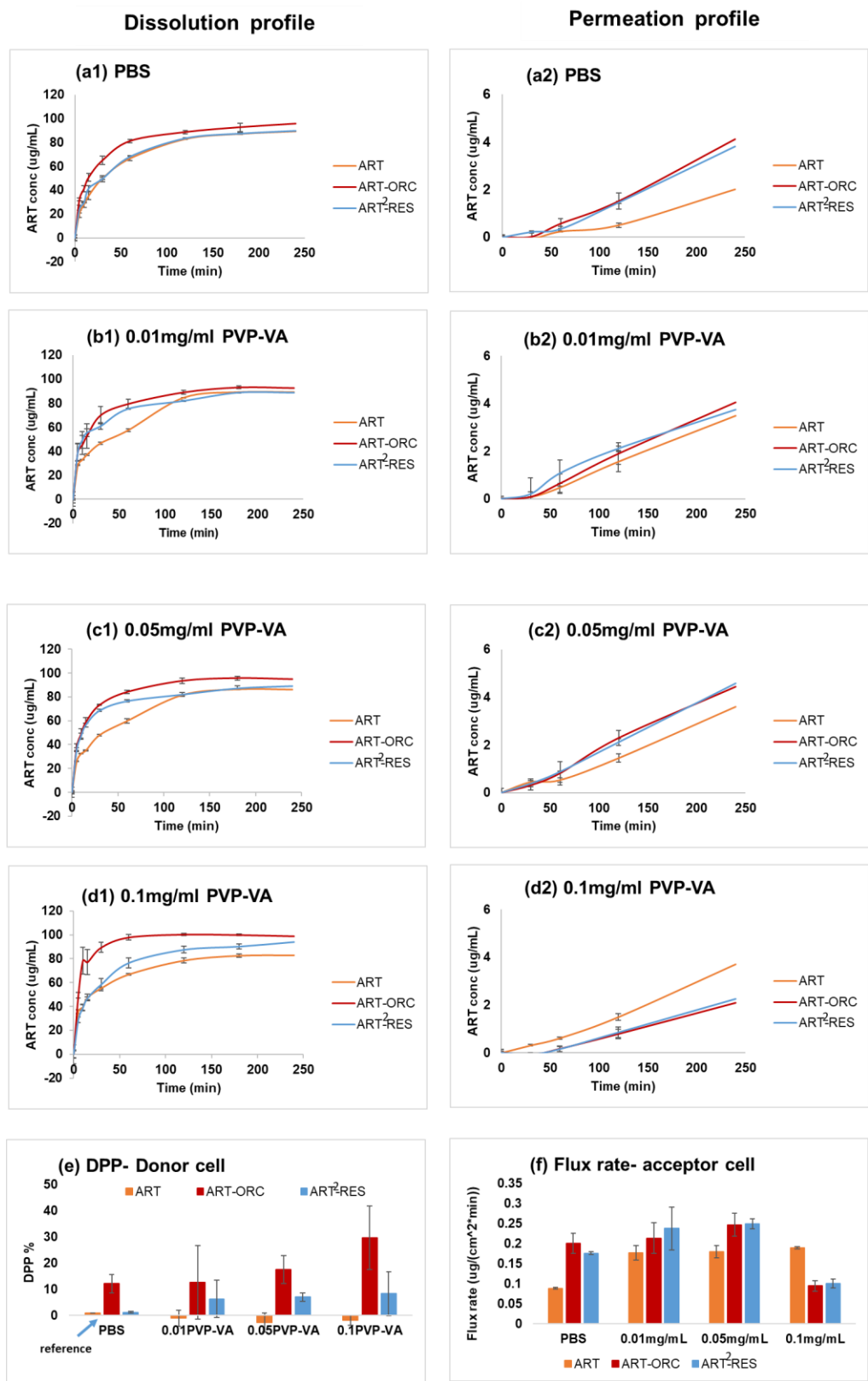


Fig. 4: Dissolution and permeation profiles of ART, ART-ORC and ART²-RES in the presence of different concentrations of PVP-VA using the D/P system: (a) PBS; (b) PBS in the presence of 0.01 mg/mL PVP-VA; (c) PBS in the presence of 0.05 mg/mL PVP-VA; (d) PBS in the presence of 0.1 mg/mL PVP-VA; (e) DPP comparison in the donor compartment; (f) flux rate comparison in the acceptor compartment.

Mechanistic understanding of the effect of the polymeric excipient on ART cocrystal dissolution and permeation properties

The roles of the selected PVP-VA in the formulation were investigated by the surface dissolution experiments of single ART cocrystals and ^1H and DOSY NMR experiments of solution including ART and coformer in either absence or presence of the polymer.

Single crystal dissolution experiments

Single crystals of ART-ORC and ART²-RES were grown using the slow evaporation approach described in the Materials and Methods section. The identities of the crystals were confirmed by PXRD measurements.

The single crystals of ART from the received materials were thin and needle-shaped. The single crystals of both ART-ORC and ART²-RES harvested were thin and brick-shaped. The representative microscopic images of these single crystals are shown in Fig. 5. The predicted morphologies of ART, ART-ORC and ART²-RES are in a good agreement with the observed images of the crystals under microscope. The predictions were further validated by comparing the measured and predicted PXRD patterns obtained from CCDC (Fig.5). It can be seen that the simulated PXRD patterns were in a good agreement with the experimental data for all crystals. The characteristic peaks of all single cocrystals were predicted quite accurately. The predicted and experimental PXRD pattern of ART was an exact match. Some mismatched peak positions in the predicted and measured PXRD patterns of ART-ORC and ART²-RES were found. The possible reason for these differences may have been the different room temperatures during the PXRD measurements. At different temperatures, the size of the unit cell is likely to be slightly different which would result in minor shifts of the PXRD peak positions.

To index the faces of single crystals used in the surface etching experiments, the face-specified PXRD measurements were carried out, which were compared with the predicted

PXRD patterns shown in Fig. 5. Based on the predicted XRD pattern of ART, the biggest face pair of (0,0,2) and (0,0, -2) showed a peak position of $2\Theta = 7.4^\circ$ in a good agreement with that of the face-specified PXRD measurement. Therefore, the (0,0,2) face of ART was indexed in the etching experiments. The pair of the biggest face (0,1,1) and (0, -1, -1) of ART-ORC showed a peak position of $2\Theta = 8.1^\circ$ in the predicted PXRD pattern, which was matched with that measured. It was concluded that the face (0,1,1) of ART-ORC was selected for etching dissolution experiments. Similarly, the (0,2,0) face of ART²-RES was determined in the etching experiment because both predicted and measured XRD patterns were matched at the peak $2\Theta = 10.1^\circ$.

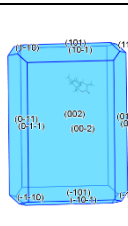
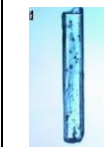
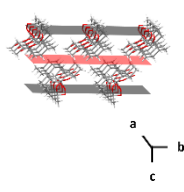
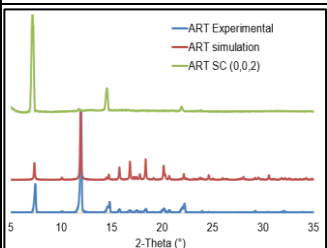
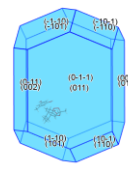

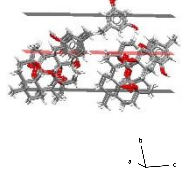
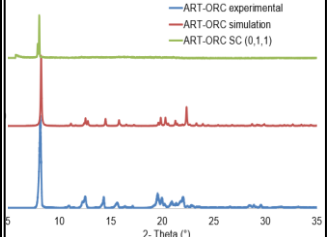
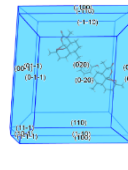

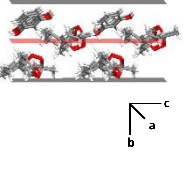
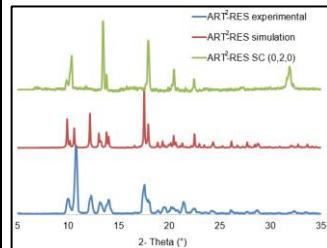
Crystal/ Reference code	Space group and packing 2D	Predicted Morphology	Experim ental morphol ogy	Face index and surface studied	XRD comparison
ART/ QNGHSU03	P2 ₁ 2 ₁ 2 ₁			(0,0,2) 	
ART-ORC CO/ TALCUG	P2 ₁ 2 ₁ 2 ₁			(0,1,1) 	
ART ² -RES CO/ TALCOA	P2 ₁			(0,2,0) 	

Fig. 5: Crystal morphology prediction and face index

The etching dissolution experiments were carried out on three single crystals of ART, ART-ORC and ART²-RES for a pre-defined time interval of 2 min (Table 2). The Raman spectroscopy results showed no change in the spectra of ART in the dissolution experiments under all conditions, i.e. the ART form remained the same Fig. 6(a). This was consistent with what was observed with SEM (Fig 7), in which no particle was seen on the crystal surfaces.

The ART characteristic peaks which did not overlap with ART-ORC peaks were at wavenumbers 2888 cm⁻¹ and 1730 cm⁻¹ [red arrows in Fig. 6(b)]. The ART-ORC characteristic peaks on the (0,1,1) face which did not overlap with the ART peaks were at wavenumbers of 2868 cm⁻¹, 1698 cm⁻¹ and 997 cm⁻¹ [green arrows in Fig. 6(b)]. The single ART-ORC cocrystal dissolution was carried out for 2 min. The Raman spectroscopy results show that, in absence of polymer (i.e. PBS alone), and in presence of pre-dissolved 0.05 mg/mL PVP-VA, characteristic peaks of both ART and ART-ORC are present, indicating precipitation of ART occurring on the ART-ORC single crystal surface. Increasing the concentration of pre-dissolved PVP-VA to 0.5 mg/mL, none of the ART characteristic peaks were observed on the measured Raman spectra in Fig. 6(b), showing that ART recrystallisation on the ART-ORC crystal surface was prevented. This conclusion was further supported by the SEM images (Fig. 7). The dissolving surface was covered by the needle shaped ART particles in PBS alone and in presence of pre-dissolved 0.05 mg/mL PVP-VA. No change was observed for the surfaces of ART-ORC in the presence of 0.5 mg/mL PVP-VA (Fig. 7), showing pits on the surface of the cocrystal.

ART²-RES CO characteristic peaks on the (0,2,0) face which did not overlap with ART peaks were at wavenumbers 2877 cm⁻¹, 1710 cm⁻¹, and 744 cm⁻¹ [green arrows in Fig. 6(c)]. The single ART²-RES cocrystal dissolution was carried out for 2 min. The Raman spectroscopy results show that in absence of polymer, i.e. PBS alone, and also in presence of

pre-dissolved PVP-VA polymer (0.05 mg/mL and 0.5 mg/mL), characteristic peaks of both ART and ART²-RES were observed in all spectra. The results showed that addition of PVP-VA in PBS did not completely prevent the ART recrystallisation on the surface of ART²-RES single cocrystal. Based on the SEM images (Fig. 7), the surfaces of ART²-RES were covered by recrystallised ART crystals in PBS alone and in presence of 0.05 mg/mL pre-dissolved PVP-VA while as the surface of ART²-RES was partially covered ART crystals in solution with 0.5 mg/mL of pre-dissolved PVP-VA.

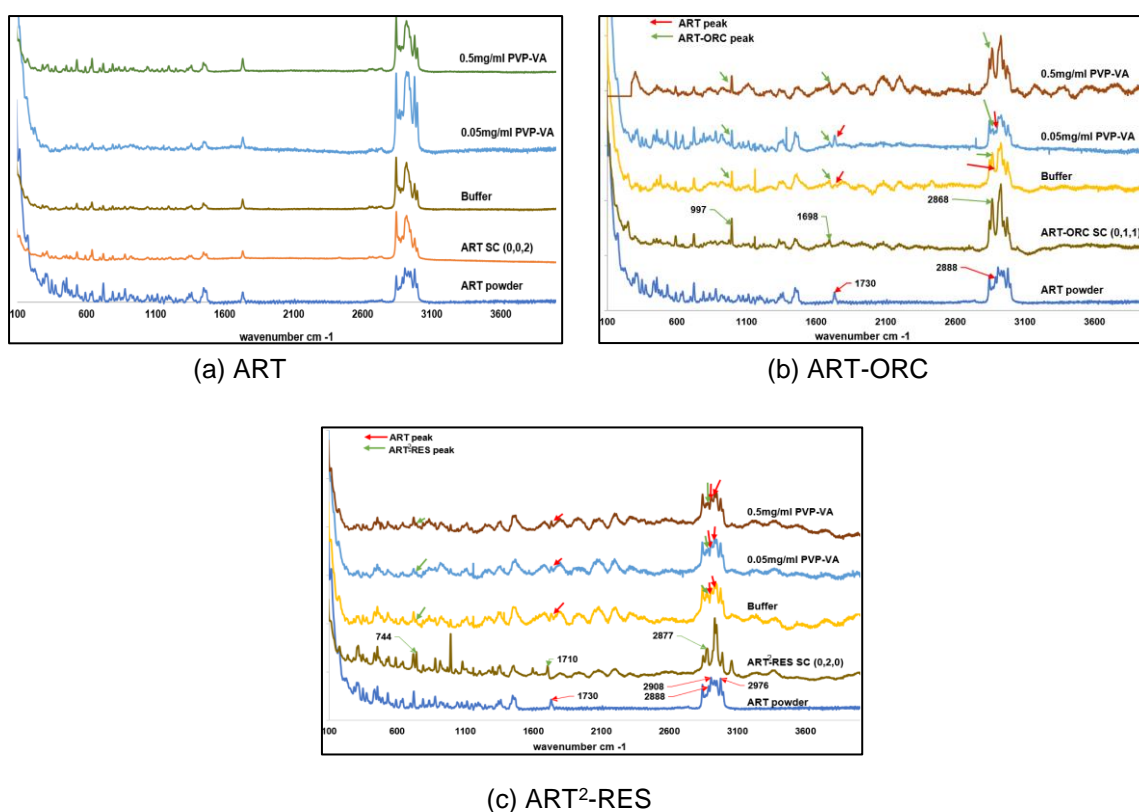


Fig. 6: Raman Spectroscopy results of the single crystal surfaces before and after etching experiments. Etching experiments were conducted on ART SC, ART-ORC SC and ART²-RES SC for 2 mins in PBS buffer in absence or presence of PVP-VA concentrations at 0.05 mg/mL or 0.5 mg/mL

	ART (0,0,2)	ART-ORC (0,1,1)	ART ² -RES (0,2,0)
Before dissolution			
PBS pH 6.8 (0.01M)			
0.05mg/mL PVP-VA			
0.5mg/mL PVP-VA			

Fig. 7: SEM graphs of crystal surfaces before and after etching experiments conducted for 2 mins in PBS buffer in absence or presence of PVP-VA concentrations of 0.05 mg/mL and 0.5 mg/mL.

Intermolecular interactions and ART diffusion properties in solution

The DOSY NMR experiments were conducted to understand the diffusion properties of ART in absence/presence of a cofomer (i.e., ORC or RES) and/or different concentrations of PVP-VA in solution. A summary of the tests in Table S3 in the Supporting Materials. Assignments of ^1H chemical shifts of ART, ORC, RES and PVP-VA were carried out previously [25-30] (detailed in Table S4 in the Supporting Materials). The focus in this study was to examine changes of the characteristic chemical shifts of the protons and diffusion coefficients, i.e., singlet peak of He closest to reactive oxygen at 5.84830 ppm and single peak at 1.43342 ppm of Ho of methyl group (Table 1) because they are sensitive to any formation of hydrogen bonding between ART with other components in solution. The full ^1H NMR spectra are given in Fig. S2 in the Supporting Materials. Effects of a cofomer and/or PVP-VA on ART in solution are not measurable from these ^1H NMR experiments (details shown in Fig. S3 in the Supporting Materials), therefore, DOSY experiments were conducted to determine the interactions between different components.

A diffusion spectrum of the sample containing ART (1mg/mL) and reference compound TMS (0.05% v/v) in CDCl_3 in Fig. 8(a) is presented as a 2D plot which has chemical shift (ppm) on the horizontal axis and D ($10^{-10} \text{ m}^2\text{s}^{-1}$) on the vertical axis. The ART (red circle) and TMS (pink circle) diffuse at different rates and are resolved in the diffusion dimension. After addition of cofomers ORC (green circle) or RES (blue circle) and PVP-VA (black circle) in solution, the change of ART diffusion coefficient can be observed in Fig. 8 (b) and Fig. 8 (c) respectively. The full DOSY NMR spectra are given in Fig. S4 in the Supporting Materials. A summary of the ART apparent diffusion coefficients D_{ART} based on the characteristic proton He in solution in the absence and presence of a cofomer and/or different concentrations of PVP-VA are shown in Table 6, where the corresponding reference compound TMS diffusion coefficient D_{TMS} in each of solutions is also given. It is clearly

shown the ART apparent diffusion coefficient D_{ART} decreases by addition of a cofomer (i.e., ORC or RES) in solution, where the diffusion coefficient D_{ART} decreases to 9.4272 (10^{-10} m^2s^{-1}) and 9.5309 (10^{-10} m^2s^{-1}) in the presence of ORC or RES respectively from the initial value of 10.3640 (10^{-10} m^2s^{-1}). This decreased diffusion coefficient D_{ART} can be directly linked to the structural properties of ART in solution through the Stokes–Einstein equation described as [31-33]

$$D_{ART} = \frac{k_B T}{6\pi\eta H_{ART}} \quad (4)$$

where k_B is the Boltzmann constant, T is the solution temperature, η is the viscosity of the solution, and H_{ART} is the effective hydrodynamics radius (i.e. Stokes radius) of ART, which is related to the size of the aggregation of ART molecules in solution.

From Eq. (4) and ART diffusion coefficients in Table 6, it was concluded that a cofomer of ORC or RES can increase the ART hydrodynamics radius, H_{ART} . In other words, the cofomers enhanced the aggregation of ART molecules in solution, which potentially led to precipitation of ART crystals. The change of ART hydrodynamic radius $\% \Delta H_{ART}$ in the presence of a cofomer and/or different concentration of PVP-VA is summarized in Table 6 (details of the calculation can be found in Supporting Materials). When ORC was added into ART solution, the hydrodynamic radius H_{ART} was increased by 2.95% and then it was reduced to 2.31% if 0.5 mg/mL PVP-VA was further added into the mixture. If 1 mg/mL PVP-VA was added in the mixture of ART and ORC, the hydrodynamic radius H_{ART} was increased just 0.77% in comparison to the ART alone solution. The same trend was found in the mixture of ART and RES. The hydrodynamic radius H_{ART} was increased by 4.42% by adding RES in the ART solution and then it was reduced to 3.79% if 0.5% PVP-VA was further added into the mixture. Adding 1 mg/mL PVP-VA in the mixture of ART and RES,

the hydrodynamic radius H_{ART} was just increased by 2.82% in comparison with the ART alone solution.

From the above analysis, it is shown that an increased PVP-VA concentration can lead to a reduced ART hydrodynamic radius $\% \Delta H_{ART}$. This may indicate a reduced possibility of precipitation of ART crystals from the cocrystal solution, showing an increased dissolution performance. This is in a good agreement with DPP results in Fig. 4(e).

A change in ART diffusion coefficient D_{ART} was evaluated further by the viscosity changes of solutions. The change of the solution viscosity $\% \Delta \eta$ in the presence of a coformer and/or different concentration of PVP-VA is summarized in Table 6 (details of the calculation can be found in Supporting Materials). When ORC was added into ART solution, the solution viscosity $\% \Delta \eta$ was increased by 6.78% and then it was reduced to -0.7% if 0.5 mg/mL PVP-VA was further added into the mixture. If 1 mg/mL PVP-VA was added in the mixture of ART and ORC, the solution viscosity $\% \Delta \eta$ was increased again to 6.63% in comparison to the ART alone solution. The same trend was found in the mixture of ART and RES. The solution viscosity $\% \Delta \eta$ was increased by 4.14% by adding RES in the ART solution and then it was reduced to 1.11% if 0.5 mg/mL PVP-VA was further added into the mixture. Adding 1 mg/mL PVP-VA in the mixture of ART and RES, the solution viscosity $\% \Delta \eta$ was just increased to 5.42% in comparison with the ART alone solution. From the analysis, it is shown that an increased PVP-VA concentration can lead to an increased the solution viscosity $\% \Delta \eta$, indicating the possibility of a reduced diffusion flux rates shown in Fig. 4(f).

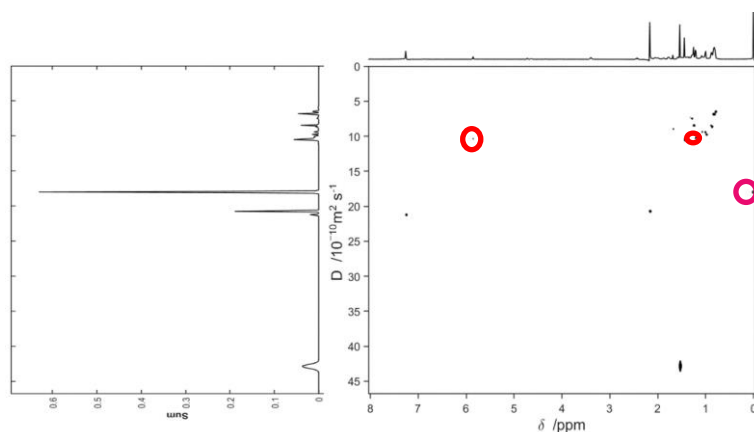
The analysis above demonstrates the profound effects of PVP-VA on the changes of ART diffusion coefficient D_{ART} within an ART cocrystal formulation, which is concentration-dependent. Therefore, optimising the concentration of PVP-VA within an ART cocrystal formulation is required during the formulation development.

A similar conclusion can be obtained from analysis of the ART diffusion coefficients D_{ART} based on the other characteristic proton H_o in solution in the absence and presence of a coformer and/or different concentrations of PVP-VA are shown in Table S5 in the Supporting Materials.

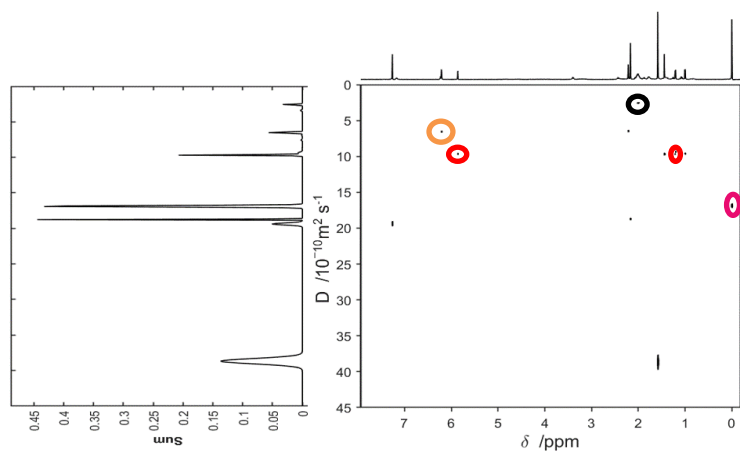
Table 6: comparison of diffusion coefficients of ART based on characteristic proton H_e

Sample	D_{ART}	D_{TMS}	$\% \Delta H_{ART}$	$\% \Delta \eta$
ART	10.3640	17.9874	0	0
1:1 ART/ORC	9.4272	16.8449	2.95	6.78
ART+ORC+ 0.5 mg/ml PVP-VA	10.2005	18.1134	2.31	-0.70
ART + ORC + 1 mg/ml PVP-VA	9.6486	16.8691	0.77	6.63
ART+ RES	9.5309	17.2728	4.42	4.14
ART+RES+ 0.5mg/ml PVP-VA	9.8755	17.7891	3.79	1.11
ART+RES +1 mg/ml PVP-VA	9.5612	17.0622	2.82	5.42

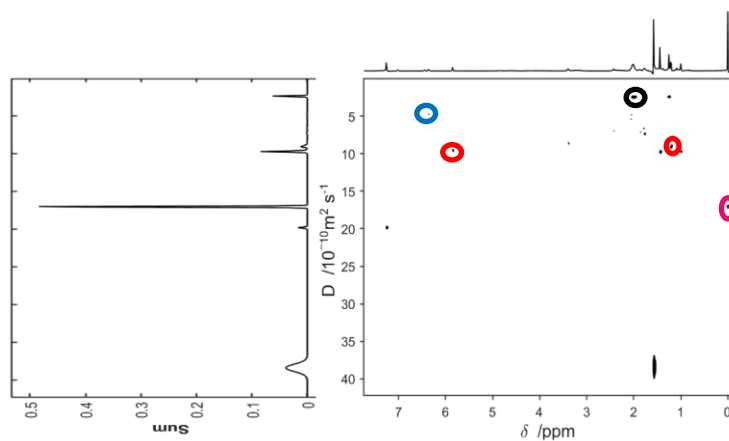
Note: 1) ART concentration in solution was 1mg/mL; 2) the change of ART hydrodynamic radius $\% \Delta H_{ART}$ is based on the reference solution of 1mg/mL ART.



(a)



(b)



(c)

Fig. 8: DOSY NMR spectra: (a) ART at 1 mg/mL in CDCl_3 ; (b) 1:1 ART: ORC in the presence of 1mg/mL PVP-VA in CDCl_3 ; (c) 2:1 ART:RES in presence of 1mg/mL PVP-VA in CDCl_3 . The diffusion coefficient analysed is circled red, green, blue and black for ART, ORC, RES and PVP-VA respectively. TMS was the reference component in CDCl_3 and circled as pink.

Discussion and conclusions

In spite of its superior antimalarial effect and good patient tolerance, the practical applications of ART are impaired by (i) poor oral activity caused by its poor solubility either in oil or water , (ii) its short-plasma half-life and, as a consequence of its poor bioavailability, (iii) the high rate of parasite recrudescence after treatment (3-5h) [4, 7]. Currently, the center of ART research is to search for new ART derivatives with higher efficacy and lower toxicity such as i.e. dihydroartemisinin, arteether, artemether, artesunate, artelinate etc. In order to deter the short plasma half-life and high recrudescence, the first-line malaria treatment recommended by World Health Organisation (WHO) is artemisinin-based combination therapies (ACTs), such as artesunate–mefloquine, artemether–lumefantrine, and dihydroartemisinin–piperaquine. The artemisinin derivatives in the combinations rapidly kill parasites but have a short half-life, which is overcome by a partner drug with a longer half-life to clear remaining parasites after the artemisinin derivative is no longer present. However, the use of ACTs in many developing countries has been severely restricted by their high costs. ART derivatives are more expensive than ART itself. For example, the cost of dihydroartemisinin used to synthesize other derivatives such as artemether and artesunate, was \$3500/kg in comparison with that ART around 180–420 US \$/kg. ART derivatives are less chemically stable with very short half-life and need a multiple dose regimen. For example, the half-life of artesunate is around 0.65 h in compared with 4.4 h of ART [5]. Therefore, developing effectively oral route of ART formulations to replace its derivatives in the treatment will significantly contribute to human wellbeing.

This is the first study, to the authors' knowledge, to explore the possibility of formulating ART cocrystals, i.e., ART-ORC and ART²-RES as oral dosage forms to deliver ART molecules to systemic circulation. The present study describes the development and evaluation of ART

cocrystal suspension formulations with PVP-VA as a crystallisation inhibitor, which will be used in *in vivo* mouse model for pre-clinical pharmacokinetic studies. It was found that ART cocrystals can increase the solubility of ART significantly, i.e. 26-fold by ART-ORC and 21-fold by ART²-RES. However, the advantages of improved ART solubility by ART cocrystals are not inherently effective; efficacy is directly related to the formulation by which cocrystals are administered. Without a crystallisation inhibitor in PBS, the ART concentrations in all three systems, i.e., ART, ART-ORC and ART²-RES, were very close to each other in the acceptor cell in the D/P experiments, indicating the potential loss of the improved solubility advantages of ART cocrystals. It was showed that the types and concentrations of the polymers significantly affected the dissolution and permeation of the ART cocrystals. In this study, PVP-VA was the most effective crystallisation inhibitor to maximize the dissolution advantages of ART cocrystals [Fig. 3(f)] and the dissolution rates of ART cocrystals can be enhanced further with increasing the concentration of PVP-VA in solution [Fig. 4(e)]. However, the flux rate of ART only increased up to a certain polymer concentration (up to 0.05 mg/mL) and then started showing a reduced flux rate in case of both cocrystals [Fig. 4(f)]. Because the absorption of oral drugs after administration is determined by the permeation of the drug molecules, the optimal concentration of PVP-VA in the formulation had to be established, i.e., 0.05 mg/mL in this study. In the meantime, a coformer of ORC or RES also affects the performance of the ART cocrystal formulation. Generally, ART-ORC showed a better performance than ART²-RES.

Surface dissolution of single ART cocrystals and diffusion properties of ART in solution, measured by ¹H and DOSY NMR measurements, were conducted to obtain a deeper understanding of the interactions between the cocrystal surface and polymer during dissolution and subsequently the interactions among ART, coformer, and polymer in solution. It was found

that PVP-VA was a good surface recrystallisation inhibitor for both ART cocrystals of ART-ORC and ART²-RES. Through prevention of ART recrystallisation on the dissolving cocrystal surfaces, the DPPs of the ART cocrystal formulations increased with a higher PVP-VA concentration [Fig. 4(e)]. However, an increased DPP of an ART cocrystal formulation does not guarantee an improved permeation profile. It was found that the flux rates of the two ART cocrystals increased with polymer concentrations of 0.01 mg/mL and 0.05 mg/mL while they decreased with 0.1 mg/mL polymer concentration [Fig. 4(f)]. The ¹H and DOSY NMR measurements revealed that a high concentration of PVP-VA can significantly reduce the hydrodynamic radius H_{ART} of the ART aggregation in Table 6, resulting in a reduced possibility of recrystallisation from solution [Fig. 4(e)]. On the other hand, an increased PVP-VA concentration can increase the solution viscosity η (Table 6). As a consequence, a higher polymer concentration could reduce the permeation rate of ART [Fig. 4(f)], although significant increase of dissolution performance of an ART cocrystal formation was observed [Fig. 4(e)]. These understandings are of essential importance in order to design an enabling cocrystal formulation. The oral absorption from a solid dosage is ultimately determined by the amount of drug molecules passing through intestinal membrane into the circulation system.

Overall, the *in vitro* study suggested the potential benefit of the developed ART cocrystal formulation as a promising drug delivery model for antimalarial therapy for bioavailability enhancement. It is worth noting that the known oral toxicity of ORC and RES are a matter of concern if these cocrystals are developed as commercial products for human use. However, this report provides a model for ART which will assist in developing cocrystals using other safer cofomers. Toxicity studies can be conducted on ORC and RES cofomers when present ART cocrystals to determine levels which could be used for human products.

ASSOCIATED CONTENT

Supporting Information

The following files are available free of charge.

Table S1: Concentrations, calibration curves and calibration validation model of ART, RES and ORC on HPLC. The concentration units are in $\mu\text{g/mL}$; Cr: real concentration of validation sample (theoretical) and Cm: measured concentration of validation sample;

Table S2: LC-MS (a) concentrations for calibration curve; (b) ART's calibration curve; (c) Validation of calibration curve (x): units in $\mu\text{g/mL}$ (for ART); Cr: real concentration of validation sample (theoretical) and Cm: measured concentration of validation sample;

Table S3: Details of NMR measurements conducted along with preparation methods;

Table S4: Summary of ^1H NMR peaks of ART, ORC, RES, and PVP-VA;

Table S5: Diffusion coefficients of ART based on characteristic proton Ho;

Fig. S1: Characterisation of ART-ORC, ART2-RES and individual components using: (a) DSC; (b) ATR-FTIR;

Fig. S2: Full ^1H NMR spectra of different components where concentrations are 1mg/mL, 0.43mg/mL and 0.19mg/mL for ART, ORC and RES respectively. The molar ratio of ART+ORC is 1:1 and ART+RES is 2:1. PVP-VA was added at concentrations of 0.5 and 1 mg/mL;

Fig. S3: comparison of the characteristic proton chemical shifts of ART at 1 mg/mL with 1:1 molar ratio of ORC or 2:1 molar ratio of RES in the presence of two different concentrations of PVP-VA: (a) single peak shift He at 5.85 ppm; (b) double-peak shifts Ho at 1.44 ppm;

Fig. S4: Full DOSY NMR spectra where concentrations are 1mg/mL, 0.43mg/mL and 0.19mg/mL for ART, ORC and RES respectively. The molar ratios are 1:1 and 2:1 for ART+ORC and ART+RES respectively. PVP-VA was added at concentrations of 0.5 and 1 mg/mL;

Detailed calculation of the percentage of change of ART hydrodynamic radius $\% \Delta H_{ART}$;

Detailed calculation of the percentage of change of viscosity of the solution $\% \Delta \eta$

Corresponding Author

Mingzhong Li – Tel: +44-1162577132; E-mail:mli@dmu.ac.uk; ORCID: 0000-0002-9532-9049; Leicester School of Pharmacy, De Montfort University, Leicester LE1 9BH, U.K.

Authors

Manreet Kaur – Leicester School of Pharmacy, De Montfort University, Leicester LE1 9BH, U.K.

Vanessa Yardley – Department of Infection & Immunity, Faculty of Infectious & Tropical Diseases, London School of Hygiene and Tropical Medicine, London, WC1E 7HT, U.K.

Ke Wang – Leicester School of Pharmacy, De Montfort University, Leicester LE1 9BH, U.K.

Jinit Masania – Leicester School of Pharmacy, De Montfort University, Leicester LE1 9BH, U.K.

Adolfo Botana – JEOL (U.K.) LTD., Welwyn Garden City, AL7 1LT, U.K.

Randolph RJ Arroo – Leicester School of Pharmacy, De Montfort University, Leicester LE1 9BH, U.K.

ACKNOWLEDGEMENTS

We would like to thank the financial support of the work by UK Engineering and Physical Sciences Research Council (EPSRC, EP/R021198/1).

Declarations of interest: The authors declare no competing financial interest.

References

1. World-Health-Organization, *World malaria report 2019*. WHO Geneva: ISBN 978-92-4-156572-1, 2019.
2. Guinovart, C., et al., *Malaria: Burden of Disease*. Current Molecular Medicine, 2006. **6**(2): p. 137-140.
3. Medhi, B., et al., *Pharmacokinetic and Toxicological Profile of Artemisinin Compounds: An Update*. Pharmacology, 2009. **84**(6): p. 323-332.
4. Chaturvedi, D., et al., *Artemisinin and its derivatives: a novel class of anti-malarial and anti-cancer agents*. Chemical Society Reviews, 2010. **39**(2): p. 435-454.
5. Ibrahim, N., et al., *Artemisinin nanoformulation suitable for intravenous injection: Preparation, characterization and antimalarial activities*. International Journal of Pharmaceutics, 2015. **495**(2): p. 671-679.
6. Aderibigbe, B.A., *Design of Drug Delivery Systems Containing Artemisinin and Its Derivatives*. Molecules (Basel, Switzerland), 2017. **22**(2): p. 323.
7. Balint, G.A., *Artemisinin and its derivatives: an important new class of antimalarial agents*. Pharmacology & Therapeutics, 2001. **90**(2): p. 261-265.
8. Shan, N., et al., *Impact of pharmaceutical cocrystals: the effects on drug pharmacokinetics*. Expert Opinion on Drug Metabolism & Toxicology, 2014. **10**(9): p. 1255-1271.
9. Qiao, N., et al., *Pharmaceutical cocrystals: An overview*. International Journal of Pharmaceutics, 2011. **419**(1-2): p. 1-11.
10. Duggirala, N.K., et al., *Pharmaceutical cocrystals: along the path to improved medicines*. Chemical Communications, 2016. **52**(4): p. 640-655.
11. Bolla, G. and A. Nangia, *Pharmaceutical cocrystals: walking the talk*. Chemical Communications, 2016. **52**(54): p. 8342-8360.
12. Karki, S., et al., *New solid forms of artemisinin obtained through cocrystallisation*. CrystEngComm, 2010. **12**(12): p. 4038-4041.
13. Babu, N.J. and A. Nangia, *Solubility Advantage of Amorphous Drugs and Pharmaceutical Cocrystals*. Crystal Growth & Design, 2011. **11**(7): p. 2662-2679.
14. Qiu, S., et al., *Role of polymers in solution and tablet-based carbamazepine cocrystal formulations*. CrystEngComm, 2016. **18**(15): p. 2664-2678.
15. Li, M., et al., *Investigation of the Effect of Hydroxypropyl Methylcellulose on the Phase Transformation and Release Profiles of Carbamazepine-Nicotinamide Cocrystal*. Pharmaceutical Research, 2014. **31**(9): p. 2312-2325.

16. Remenar, J.F., et al., *Celecoxib:Nicotinamide Dissociation: Using Excipients To Capture the Cocrystal's Potential*. *Molecular Pharmaceutics*, 2007. **4**(3): p. 386-400.
17. Qiao, N., et al., *In situ monitoring of carbamazepine–nicotinamide cocrystal intrinsic dissolution behaviour*. *European Journal of Pharmaceutics and Biopharmaceutics*, 2013. **83**(3): p. 415-426.
18. Childs, S.L., P. Kandi, and S.R. Lingireddy, *Formulation of a Danazol Cocrystal with Controlled Supersaturation Plays an Essential Role in Improving Bioavailability*. *Molecular Pharmaceutics*, 2013. **10**(8): p. 3112-3127.
19. Guo, M., et al., *Investigating the Influence of Polymers on Supersaturated Flufenamic Acid Cocrystal Solutions*. *Molecular Pharmaceutics*, 2016. **13**(9): p. 3292-3307.
20. Guo, M., et al., *Investigating Permeation Behavior of Flufenamic Acid Cocrystals Using a Dissolution and Permeation System*. *Molecular Pharmaceutics*, 2018. **15**(9): p. 4257-4272.
21. Guo, M., et al., *Insight into Flufenamic Acid Cocrystal Dissolution in the Presence of a Polymer in Solution: from Single Crystal to Powder Dissolution*. *Molecular Pharmaceutics*, 2017. **14**(12): p. 4583-4596.
22. Kirubakaran, P., et al., *Understanding the Effects of a Polymer on the Surface Dissolution of Pharmaceutical Cocrystals Using Combined Experimental and Molecular Dynamics Simulation Approaches*. *Molecular Pharmaceutics*, 2020. **17**(2): p. 517-529.
23. Good, D.J. and N. Rodríguez-Hornedo, *Solubility Advantage of Pharmaceutical Cocrystals*. *Crystal Growth & Design*, 2009. **9**(5): p. 2252-2264.
24. Sahoo, N.G., et al., *Preparation, characterization and dissolution behavior of artemisinin microparticles*. *Advanced Powder Technology*, 2011. **22**(4): p. 458-463.
25. Blaskó, G., G.A. Cordell, and D.C. Lankin, *Definitive 1H- and 13C-nmr Assignments of Artemisinin (Qinghaosu)*. *Journal of Natural Products*, 1988. **51**(6): p. 1273-1276.
26. Castilho, P.C., S.C. Gouveia, and A.I. Rodrigues, *Quantification of artemisinin in Artemisia annua extracts by 1H-NMR*. *Phytochemical Analysis*, 2008. **19**(4): p. 329-334.
27. Jørgensen, S.H., et al., *Fusarium graminearum PKS14 is involved in orsellinic acid and orcinol synthesis*. *Fungal Genetics and Biology*, 2014. **70**: p. 24-31.
28. Monde, K., et al., *Organochlorine Compounds from a Terrestrial Higher Plant: Structures and Origin of Chlorinated Orcinol Derivatives from Diseased Bulbs of Lilium maximowiczii*. *Journal of Natural Products*, 1998. **61**(7): p. 913-921.
29. Gosecki, M., et al., *Influence of Glycoluril Molecular Clip Isomerization on the Mechanisms of Resorcinol Molecule Complexation*. *The Journal of Physical Chemistry C*, 2020. **124**(15): p. 8401-8410.
30. Ma, J.-h., et al., *Interaction of Urea with Pluronic Block Copolymers by 1H NMR Spectroscopy*. *The Journal of Physical Chemistry B*, 2007. **111**(19): p. 5155-5161.
31. Cohen, Y., L. Avram, and L. Frish, *Diffusion NMR Spectroscopy in Supramolecular and Combinatorial Chemistry: An Old Parameter—New Insights*. *Angewandte Chemie International Edition*, 2005. **44**(4): p. 520-554.
32. Avram, L. and Y. Cohen, *Diffusion NMR of molecular cages and capsules*. *Chemical Society Reviews*, 2015. **44**(2): p. 586-602.
33. Brand, T., E.J. Cabrita, and S. Berger, *Intermolecular interaction as investigated by NOE and diffusion studies*. *Progress in Nuclear Magnetic Resonance Spectroscopy*, 2005. **46**(4): p. 159-196.